Fast Fluid Antenna Multiple Access With Path Loss Consideration and Different Antenna Architecture

1st Halvin Yang
Department of Electronic and Electrical Engineering
University College London (UCL)
London, United Kingdom
uceehhy@ucl.ac.uk

2nd Xiao Lin
School of Information and Communication Engineering
University of Electronic Science and Technology of China (UESTC)
Chengdu, China
xiaolin_uestc@163.com

3rd Kai-Kit Wong
Department of Electronic and Electrical Engineering
University College London (UCL)
London, United Kingdom
kai-kit.wong@ucl.ac.uk

4th Yizhe Zhao
School of Information and Communication Engineering
University of Electronic Science and Technology of China (UESTC)
Chengdu, China
Corresponding Author, yzzhao@uestc.edu.cn

***Abstract*—Fluid antennas is able to exploit the natural characteristic of multipath propagation and randomness of the wireless channel by adjusting the port position spatially for improving the signal strength. In a fast fluid antenna multiple access (f-FAMA) system, multiple user devices (UDs) are all equipped with the fluid antenna for mitigating the impact of interference, in order to reduce the outage probability and increase the multiplexing gain. Previous works have established a wireless channel model for such a f-FAMA system by considering the relevance among different ports. In this paper, an improved version of the wireless channel model is proposed by also taking into account the path loss difference among different ports. The impact of different fluid antenna architectures on the performance of the f-FAMA system is also investigated. Simulation results demonstrate the necessity of considering path loss variations, particularly in scenarios where the fluid antenna has a larger size. Additionally, among three different antenna architectures discussed in this paper, the linear and the circular topology outperform the wheel topology in the case of a shorter reference distance.**

***Index Terms*—Fluid antenna, Multiple Access, Performance Analysis, Path Loss, Antenna Architecture**

I. Introduction

The increasing requirement of massive connectivity is posing a challenge on the multiple-access in mobile communications, where a projected 30 billion more edge devices is expected to swarm into the network by 2030 [1]. It is essential for us to resort to some new technologies, which can accommodate a large number of users in the resource-limited network. Multiple-input multiple-output (MIMO) technology [2] has been studied for years, which is capable of leveraging the spatial diversity to enhance the communication efficiency, while an even greater connectivity can be then achieved with the aid of massive MIMO [3]. To further increase the capacity beyond this, non-orthogonal multiple-access (NOMA) technology [4] has also been tipped to play a significant role in future wireless communications, thanks to it's capability for enabling user devices (UDs) to cope with the problem of interference.

Despite the merits of NOMA and MIMO, the lack of scalability restrict them to be adopted in a more wide scenario. NOMA requires accurate multiuser detection at the user devices, which could put a strain on the limited computational resources available - current analysis often limits NOMA to two co-channel users only. Furthermore, MIMO requires the knowledge of the channel state information (CSI) at the base station, which increases the complexity of the system, not to mention the high energy and hardware cost of using multiple active antennas. Ideally, the multiple access technology should not have its complexity rise with the increase of UDs and does not require such high processing power that UDs will be overloaded.

An emerging technology that may be the key to rectifying these shortcomings are fluid antennas, which has potential to be one of the key technologies for 6G. Fluid antennas represent any radiating structure that can change its position on demand to any one of a predetermined locations, namely ports. In practise, it can be a reconfigurable pixel-based antenna [5]–[7] or a conductive/dielectric liquid-based antenna [8]–[10].

The first analysis of fluid antennas in a communication system was proposed by Wong *et al* in [11]. With the aid of a software-controlled antenna that can instantaneously switch locations in space, it is possible to access the fading envelopes at different locations and select the best port with the largest signal to interference and noise ratio (SINR). Since the fluid antenna is taking advantage of natural multipath fading and mitigating the impact of interference, no complex pre-processing or pre-coding of the signals is required. Since the port selection is based on the signal power at each port, the acquisition of CSI at the BS is not required anymore. The usage of fluid antennas in mobile communications has been explored in both single user [11]–[17] and multi-user [18]–[21] scenarios.

Of particular relevance to this paper is the ability for a fluid antenna system (FAS) to deal with co-channel interference in

a multi-user scenario. There are two fluid antenna multiple access (FAMA) schemes, namely slow FAMA (s-FAMA) and fast FAMA (f-FAMA). s-FAMA assumes the channel is constant within a certain time frame by only switching the active port whenever the channel envelope changes, which has been confirmed to have the ability to support multiple users (< 6) in the same channel [19]. Although s-FAMA is a simple paradigm to be realized in practical scenarios, it is far from achieving the desired massive connectivity. Therefore, fast FAMA (f-FAMA), which switches the location of the active antenna on a symbol-by-symbol basis, has been shown to be capable of enabling massive connectivity with tens or hundreds of UDs by having a single fluid antenna present at each UD [18]. However, the challenges with switching ports in coordination with every symbol instance are twofold. The mechanical ability of the fluid antenna to switch locations every symbol (which would be several thousand times per second) is not yet feasible with current technology, and the high computational load for calculating the optimal port in every symbol duration would not be possible for many UDs having limited computational resources.

To address this issue, [20] provides an algorithm for port selection of f-FAMA, where each UD has no prior information about channel statistics or interferers and only has access to the knowledge of the fading envelopes of its own channel. In order to achieve port selection under such conditions, the paper attempts to estimate the sum of the interference and noise power present at each port of the UD by recognizing that the sum of the interference and noise power should be uncorrelated with the UD's own channel. Therefore, by using a series of cross-correlation and similarity metrics, the estimation with the lowest correlation to the channel power is achieved.

Path loss is an important coefficient in wireless channels, which degrades the receive signal power seriously. [22] provides several path loss models based around real world 28GHz and 73GHz measurements. Both a LoS and nLoS path loss model is derived, with the LoS using a free-space probabilistic approach and the nLoS model using a floating intercept model. [23] takes a closer look at analysis of path loss in urban scattering environments for lower frequencies (5.85GHz), considering the penetration of houses and trees.

However, existing works studying FAMA do not considered the path loss difference among the ports of the fluid antennas. Therefore, this paper expands on the work in [20] by detailing the path loss of each port of FAS to provide a more accurate channel model. Since the Rician channel model is considered in this paper, both the LoS and nLoS elements exist and a simple free-space reference distance path loss model outlined in [22] is conceived. Then, a method for modelling the distance from the transmit antenna of the BS to every single port of the FAS is proposed. The affect of path loss consideration is evaluated via the outage probability and multiplexing gain of the system.

Moreover, the architecture of the fluid antennas also impacts the performance of the FAMA system. In this paper, the linear, circular and wheel architectures of fluid antenna presented in [13] are investigated. Different architectures result in different inter-ports distance as well as different transmitter-ports distance, which further affects the corresponding path loss and in turn has an impact on the overall performance of the f-FAMA system. Aside from path loss consideration, the 2D layout of the ports also has an effect on the correlation between each port as well as the way interference signals interact, changing the overall channel envelope. The outage probability is selected as the metric for evaluating the FAMA performance by adopting different fluid antenna architectures.

Although earlier work attempted to give a closed form solution to performance indicators like outage probability [11], [18], it has been shown that due to the correlation between different ports on the FAS that the outage probability in multi-user scenarios and even complex single-user scenarios is in such a form to prevent the obtaining of a simple expression. Papers like [21] attempted to get around this issue by using approximations like the Gaussian approximation via the central limit theorem, however there were inaccuracies involved with the estimation. In order to limit the inaccuracies from mathematical estimates, this paper will directly use Monte Carlo simulations instead of giving a closed form mathematical expression when providing results.

To summarise, the contributions in this paper are summarized as follows:

- We derive a more accurate channel model by considering the path loss difference among different ports on the FAS. The performance of this new model is then compared to the previous model to identify the significance of path loss.
- The outage probability and the multiplexing gain of the f-FAMA system are analysed by considering different architectures of fluid antenna. Simulation results also compares the performance of different fluid antenna architectures.

Section II provides the system model with path loss and different fluid antenna architecture consideration as well as providing the performance indicator, in this case the outage probability expression. Section III looks in depth at obtaining the channel model for each fluid antenna architecture and Section IV show the performance analysis results. Finally this paper is concluded in Section V.

II. F-FAMA System with Path Loss Consideration

A. System Model With Path Loss Consideration

As illustrated in Fig. 1, a f-FAMA system is studied, which consists of a single base station and a total of U UDs each equipped with a single N-port fluid antenna of size $W\lambda$, where λ is the wavelength. The BS has a total of U antennas, with each antenna being in charge of transmitting one UD's signal to the intended UD. It is assumed that there is one direct line-of-sight (LoS) and a total of N_p non line-of-sight (nLoS) paths caused by scatterers present in the wireless environment. Therefore, according to [20], the received signal at the k-th port of the u-th UD can be expressed as

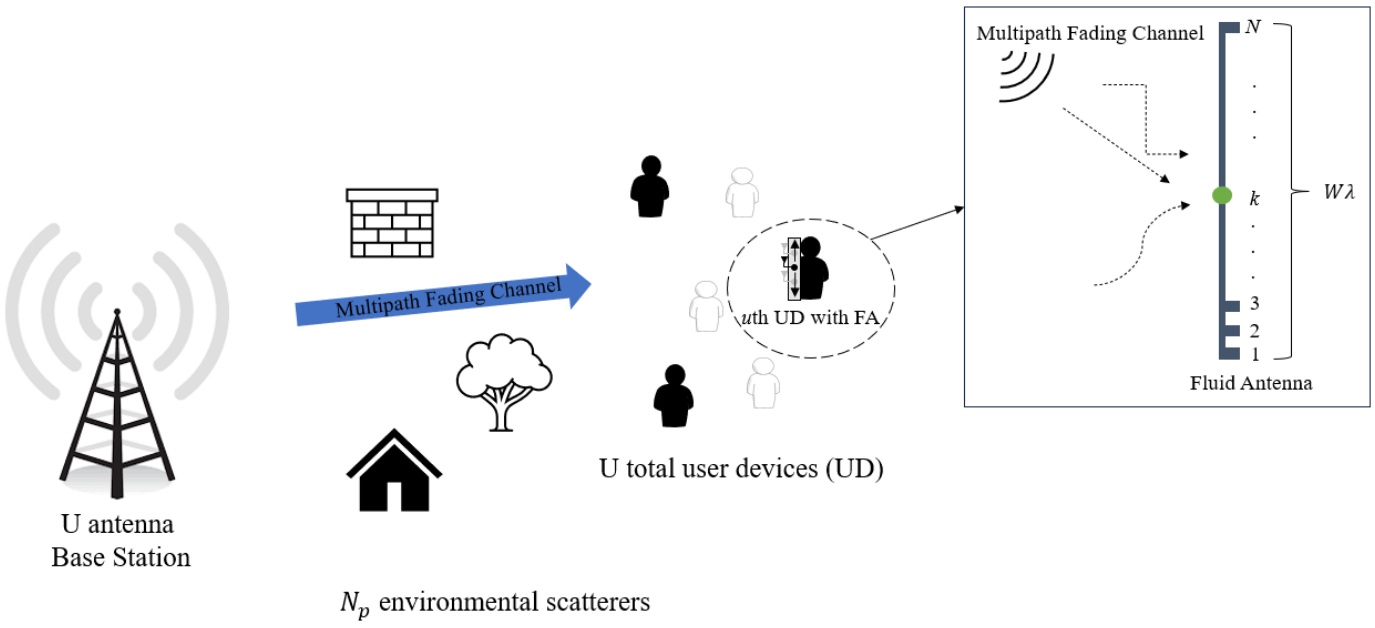

Fig. 1: System model of the f-FAMA system.

$$r_k^{(u)} = g_k^{(u,u)} s_u + \sum_{\tilde{u}\neq u}^{U} g_k^{(\tilde{u},u)} s_{\tilde{u}} + \eta_k^{(u)}, \tag{1}$$

where $g_k^{(\tilde{u},u)}$ is the channel gain between the $\tilde{u}$-th transmit antenna at the base station and the k-th port of the u-th UD, s_u is the information symbol transmitted to the u-th UD having a power of $\mathbb{E}[|s_u|^2] = \sigma_s^2$ and $\eta_k^{(u)}$ is the zero-mean additive white gaussian noise (AWGN) having a variance of σ_η^2 at the k-th port of the u-th UD . According to [20], the channel gain $g_k^{(\tilde{u},u)}$ which consists of a LoS component and N_p nLoS components can be expressed as

$$g_k^{(\tilde{u},u)} = \sqrt{\frac{Kp_k}{K+1}} e^{j\alpha^{(\tilde{u},u)}} e^{-j\frac{2\pi d_k}{\lambda} sin\theta_0^{(\tilde{u},u)} cos\phi_0^{(\tilde{u},u)}} + \sum_{l=1}^{N_p} a_l^{(\tilde{u},u)} e^{-j\frac{2\pi d_k}{\lambda} sin\theta_l^{(\tilde{u},u)} cos\phi_l^{(\tilde{u},u)}}, \tag{2}$$

where K is the Rice factor. $p_k = D_k^{-\beta}$ is the path loss for the k-th channel, where D_k represents the distance from the transmitter to the k-th port of UD and β is the path loss exponent. d_k is the displacement of the k-th port, $\alpha^{(\tilde{u},u)}$ is the random phase of the specular component and $a_l^{(\tilde{u},u)}$ is the random complex coefficient of the l-th multipath, where $\mathbb{E}[\sum_l |a_l^{(\tilde{u},u)}|^2] = \frac{p_k}{K+1}$. The azimuth angle of arrival (AoA) and elevation AoA are denoted as θ and ϕ, respectively. Note that the angle of departure (AoD) of the base station is not considered due to base station antennas being far apart from each other and experience different scatterers in the environment.

B. Performance Indicators

Similar to [20], this paper analyses the outage probability of the f-FAMA system. In order to obtain the SINR, the optimal port must be selected firstly by identifying the port at which the SINR is the highest, which is expressed as

$$k^* = arg\max_k \frac{|g_k^{(u,u)} s_u|^2}{|\sum_{u=1}^{U}\sum_{\tilde{u}\neq u} g_k^{(\tilde{u},u)} s_{\tilde{u}} + \eta_k^{(u)}|^2} = arg\max_k \frac{|g_k^{(u,u)}|^2}{|\tilde{g}_k^{(u)}|^2}, \tag{3}$$

where s_u and $s_{\tilde{u}}$ disappear because the signal power is constant across all ports. Although the process of port selection may look similar to traditional antenna selection systems, there are some key differences. Most notably, multiple fixed antennas require a spacing of at least $\frac{\lambda}{2}$ to maintain diversity whereas ports on a fluid antenna should be as close as possible to increase the spatial resolution. Furthermore, a selection combining system with L antennas will still require L radio frequency (RF) chains, while a fluid antenna with N ports only requires a single RF chain.

The performance of each UD can be then characterised using outage probability, which is the probability that the highest SINR among all the ports is lower than a threshold γ.

$$p_{out}^{(u)} = Prob\left(\max_k \frac{|g_k^{(u,u)}|^2}{|\tilde{g}_k^{(u)}|^2} < \gamma\right). \tag{4}$$

Without loss of generality, we assume that all the user devices have identical channel statistics. Then, the multiplexing gain of the f-FAMA system is formulated as

$$m = U(1 - p_{out}^{(u)}). \tag{5}$$

III. Different Fluid Antenna Architectures

In the previous section, a new channel model with path loss consideration is proposed. However, the different architectures considered will inevitably lead to the difference in the distances from the transmitter to each port and thereby resulting in variations in the path loss. Additionally, different architectures also result in different expressions d_k of the displacement of the k-th port. Therefore, it's of great importance to derive the expression of $g_k^{(\tilde{u},u)}$ for different antenna architectures. Without loss of generality, the linear, circular and wheel architectures [13] are considered.

The following subsections give the derivations of the channel based on different antenna topologies. First, the distance between the reference and kth port is obtained (d_k), then the path loss is calculated by first deriving an expression for the distance between the kth port and the transmit antenna (D_k).

A. Linear Architecture

In the linear architecture of FAS, the displacement (i.e. the Euclidean distance) at the k-th port from the first one is given by

$$d_k = \frac{k-1}{N-1} W\lambda. \tag{6}$$

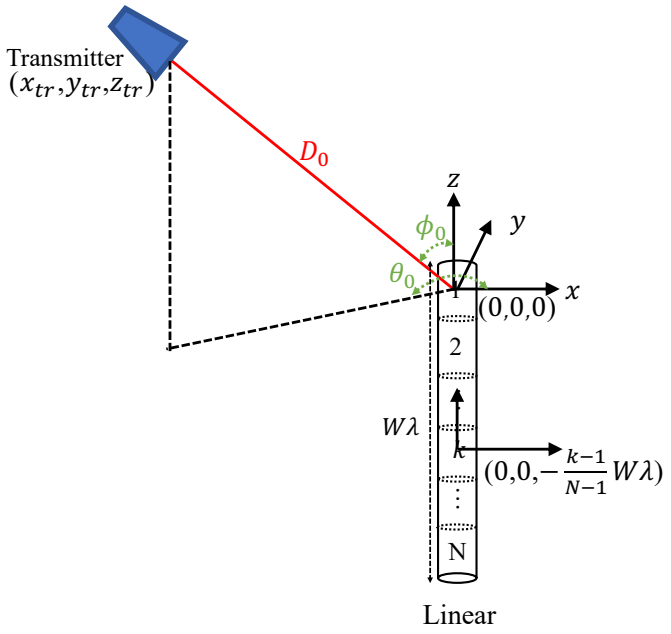

Fig. 2: FAS with the linear architecture.

Assume that the port 1 is the reference port and the coordinate of port 1 is $(0,0,0)$. From Fig. 2, we can obtain the position of the transmitter as

$$\begin{cases} x_{tr} = D_0 \sin\phi_0^{(\tilde{u},u)} \cos\theta_0^{(\tilde{u},u)} \\ y_{tr} = D_0 \sin\phi_0^{(\tilde{u},u)} \sin\theta_0^{(\tilde{u},u)} \\ z_{tr} = D_0 \cos\phi_0^{(\tilde{u},u)} \end{cases} \tag{7}$$

where D_0 represents the distance between the transmitter and the reference port. Therefore, the distance between the transmitter and other ports can be obtained as

$$\begin{aligned} D_k &= \sqrt{x_{tr}^2 + y_{tr}^2 + (z_{tr} - d_k)^2} \\ &= \sqrt{D_0^2 + d_k^2 - 2D_0 d_k \cos\phi_0^{(\tilde{u},u)}} \\ &= \sqrt{D_0^2 + \frac{k-1}{N-1} W\lambda (\frac{k-1}{N-1} W\lambda - 2D_0 \cos\phi_0)} \end{aligned} \tag{8}$$

Therefore, eq.(2) can be rewritten as

$$\begin{aligned} g_k^{(\tilde{u},u)} =& \sqrt{\frac{Kp_k}{K+1}} e^{j\alpha^{(\tilde{u},u)}} e^{-j\frac{2\pi(k-1)W}{N-1}\sin\theta_0^{(\tilde{u},u)}\cos\phi_0^{(\tilde{u},u)}} \\ &+ \sum_{l=1}^{N_p} a_l^{(\tilde{u},u)} e^{-j\frac{2\pi(k-1)W}{N-1}\sin\theta_l^{(\tilde{u},u)}\cos\phi_l^{(\tilde{u},u)}} \end{aligned} \tag{9}$$

where $p_k = D_k^{-\beta}$. The calculation formula for D_k is given by eq.(8).

B. Circular Architecture

In the circular architecture of FAS, the displacement (i.e. the Euclidean distance) at the k-th port from the port 1 is given by

$$d_k = \sin(\frac{k-1}{N}\pi) W\lambda \tag{10}$$

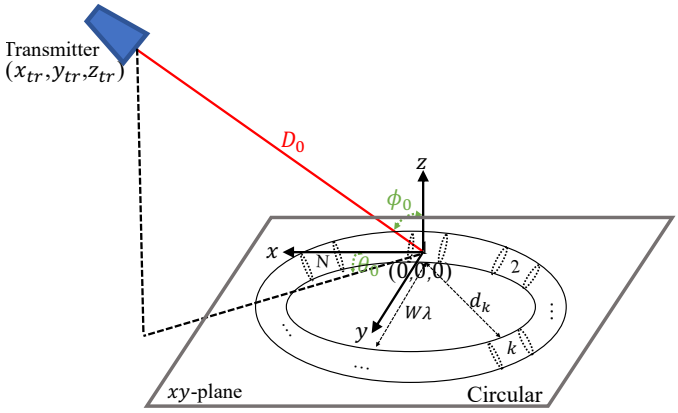

Fig. 3: FAS with the circular architecture.

The port 1 of the circular FAS is defined as the reference port, whose coordinates is $(x_1, y_1, z_1) = (0,0,0)$, which is illustrate in Fig. 3. We first obtain the x-coordinate of the remaining ports as

$$x_k^{(\tilde{u},u)} = \begin{cases} \frac{d_k\sqrt{(W\lambda)^2 - d_k^2}}{W\lambda}, & k \le \lfloor N/2 \rfloor + 1 \\ -\frac{d_k\sqrt{(W\lambda)^2 - d_k^2}}{W\lambda}, & else \end{cases} \tag{11}$$

where $\lfloor\rfloor$ represents rounding down operation. Similarly, the y-coordinate and the z-coordinate of the remaining ports are obtained as $y_k^{(\tilde{u},u)} = \frac{d_k^2}{W\lambda}$ and $z_k^{(\tilde{u},u)} = 0$, respectively. Further,

the distance between the transmitter and other ports is obtained as

$$D_k = \sqrt{(x_{tr} - x_k^{(\tilde{u},u)})^2 + (y_{tr} - y_k^{(\tilde{u},u)})^2 + (z_{tr} - z_k^{(\tilde{u},u)})^2} \tag{12}$$

According to (11), we have

$$D_k = \begin{cases} \sqrt{C_1}, & k \leq \lfloor N/2 \rfloor + 1 \\ \sqrt{C_2}, & else \end{cases} \tag{13}$$

where

$$\begin{aligned} C_1 &= D_0^2 + d_k^2 - \frac{2D_0 d_k \sin\phi_0^{(\tilde{u},u)}}{W\lambda}(d_k \sin\theta_0^{(\tilde{u},u)} \\ &\quad + \sqrt{(W\lambda)^2 - d_k^2}\cos\theta_0^{(\tilde{u},u)}) \\ C_2 &= D_0^2 + d_k^2 - \frac{2D_0 d_k \sin\phi_0^{(\tilde{u},u)}}{W\lambda}(d_k \sin\theta_0^{(\tilde{u},u)} \\ &\quad - \sqrt{(W\lambda)^2 - d_k^2}\cos\theta_0^{(\tilde{u},u)}) \end{aligned} \tag{14}$$

Then, the new channel model can be expressed by

$$\begin{aligned} g_k^{(\tilde{u},u)} =& \sqrt{\frac{Kp_k}{K+1}} e^{j\alpha^{(\tilde{u},u)}} e^{-j2\pi \sin(\frac{k-1}{N}\pi) W \sin\theta_0^{(\tilde{u},u)} \cos\phi_0^{(\tilde{u},u)}} \\ &+ \sum_{l=1}^{N_p} a_l^{(\tilde{u},u)} e^{-j2\pi \sin(\frac{k-1}{N}\pi) W \sin\theta_l^{(\tilde{u},u)} \cos\phi_l^{(\tilde{u},u)}} \end{aligned} \tag{15}$$

where $p_k = D_k^{-\beta}$. The calculation formula for D_k is given by eq.(13).

C. Wheel Architecture

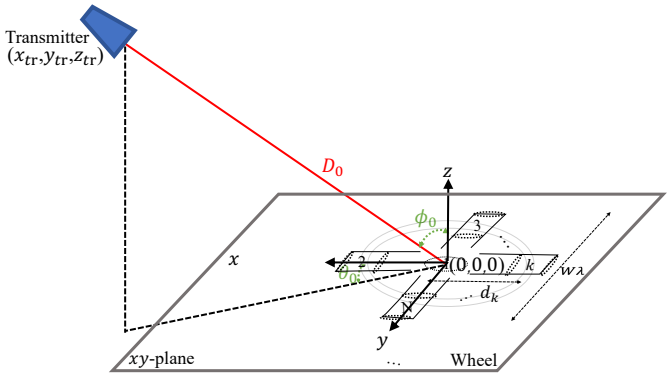

Fig. 4: FAS with the wheel architecture.

In the wheel architecture of the FAS, we have

$$d_k = \mathbb{1}_{k>1} \frac{W\lambda}{2}. \tag{16}$$

By assuming all ports are evenly distributed, the angle between each port is given as

$$\delta = \frac{2\pi}{N-1} \tag{17}$$

where N represents the number of ports and port numbers increase sequentially. We establish a coordinate system (Figure 4) with port 1 as the origin of coordinates, while the direction pointing to port 2 is defined as the x-axis. Then, the x-coordinate and the y-coordinate of the remaining ports are obtained as

$$\begin{cases} x_k = d_k \cos((k-2)\delta) \\ y_k = -d_k \sin((k-2)\delta) \\ z_k = 0 \end{cases} \tag{18}$$

Therefore, the distance between the base station and the ports can be expressed as

$$\begin{aligned} D_k &= \sqrt{(x_{tr} - x_k^{(\tilde{u},u)})^2 + (y_{tr} - y_k^{(\tilde{u},u)})^2 + (z_{tr} - z_k^{(\tilde{u},u)})^2} \\ &= \{D_0^2 + d_k^2 - 2D_0 \sin\phi_0 d_k [\cos\theta_0 \cos\frac{2\pi(k-2)}{N-1} \\ &\quad - \sin\theta_0 \sin\frac{2\pi(k-2)}{N-1}]\}^{\frac{1}{2}} \\ &= \{D_0^2 + \frac{\lambda^2}{4} - 2D_0 \sin\phi_0 \frac{\lambda}{2} [\cos\theta_0 \cos\frac{2\pi(k-2)}{N-1} \\ &\quad - \sin\theta_0 \sin\frac{2\pi(k-2)}{N-1}]\}^{\frac{1}{2}} \end{aligned} \tag{19}$$

The new channel model is then expressed as

$$\begin{aligned} g_k^{(\tilde{u},u)} =& \sqrt{\frac{Kp_k}{K+1}} e^{j\alpha^{(\tilde{u},u)}} e^{-j2\pi \mathbb{1}_{k>1} \frac{W}{2} \sin\theta_0^{(\tilde{u},u)} \cos\phi_0^{(\tilde{u},u)}} \\ &+ \sum_{l=1}^{N_p} a_l^{(\tilde{u},u)} e^{-j2\pi \mathbb{1}_{k>1} \frac{W}{2} \sin\theta_l^{(\tilde{u},u)} \cos\phi_l^{(\tilde{u},u)}} \end{aligned} \tag{20}$$

where $p_k = D_k^{-\beta}$. The calculation formula for D_k is given by eq.(19).

IV. Simulation Results

In this section, we evaluate the performance of the f-FAMA system with the aid of Monte Carlo based simulation, by adopting the proposed channel model with path loss consideration and the model in [20], respectively. Then, the performance differences of fluid antennas with different topologies are also evaluated. The channel models of three topologies have been described in Eq.(8), Eq.(14) and Eq.(20). We define the signal-to-noise-ratio (SNR) as $\Gamma = \sigma_s^2/\sigma_\eta^2$, which is set to 10 dB. Without specific statement, we set $(K, Np) = (7, 2)$, $\mathbb{E}[|s_u|^2] = 1$ and the SINR threshold of outage is set to $\gamma = 10$ dB.

Fig. 5 illustrates the the outage probability versus the reference distance D_0 by considering two channel models (with or without path loss consideration) with different Angle of Arrival (AoA). Generally, when we increase the reference distance, the outage probability also increases, since the path loss becomes more serious at a longer transmission distance. We consider two extreme cases: $\phi_0^{(\tilde{u},u)} = 0$ and $\phi_0^{(\tilde{u},u)} = \pi$. When $\phi_0^{(\tilde{u},u)} = 0$, $D_k = D_0 - d_k$, and when $\phi_0^{(\tilde{u},u)} = \pi$,

$D_k = D_0 + d_k$. Observe from Fig. 5 that the performance of $\phi_0^{(\tilde{u},u)} = 0$ is superior to that of $\phi_0^{(\tilde{u},u)} = \pi$. This is attributed to the reduction in distance from the transmitter to the k-th port of the UD, which results in a non-negligible decreasing in path loss. This confirms the importance of taking into account the difference of path loss and the Angle of Arrival (AoA) from the transmitter to the different ports.

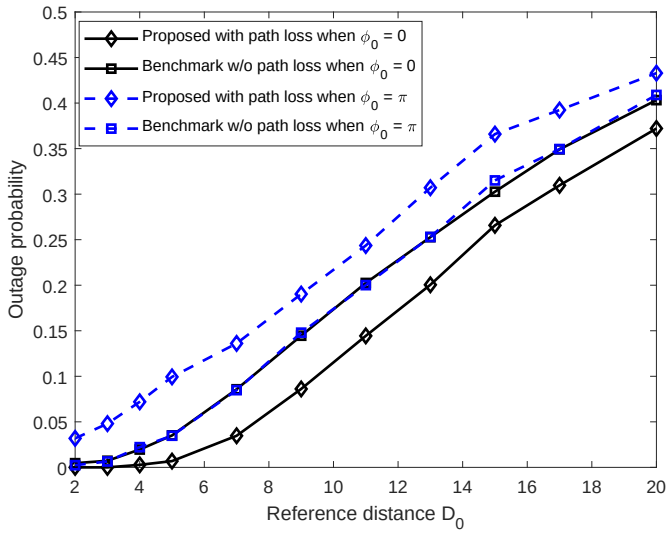

Fig. 5: Outage probability versus the reference distance D_0 by considering two channel models (with or without pass loss consideration), when $N = 600$, $U = 6$, and $W = 30$.

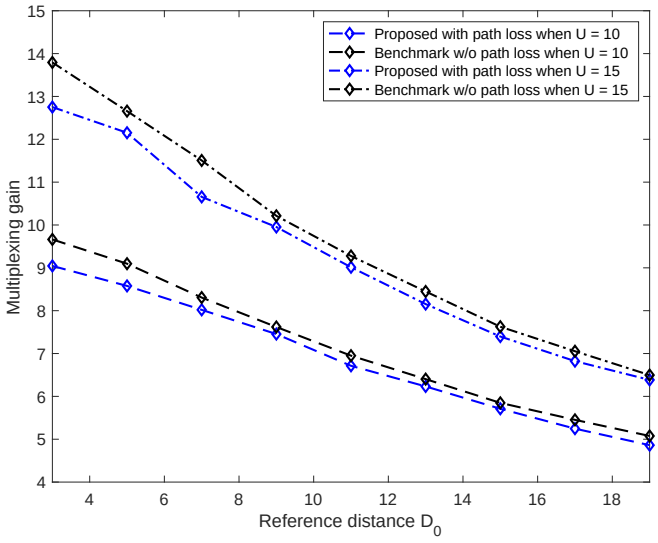

Fig. 6: Multiplexing gain versus the reference distance D_0 by considering two channel models (with or without pass loss consideration), when $N = 600$, and $W = 25$.

Fig. 6 depicts the multiplexing gain versus the reference distance by setting different UD numbers. Observe from Fig. 6 that the multiplexing gain reduces when we increase D_0, since the more serious path loss results in a higher outage probability. Concurrently, when the number of users $U = 15$, the performance of the f-FAMA system deteriorates notably faster as the distance increases, compared to the scenario with $U = 10$. This is because a larger UD number results in a more serious interference. Moreover, the new channel model considering the path loss difference shows a slightly lower performance compared to the old channel model.

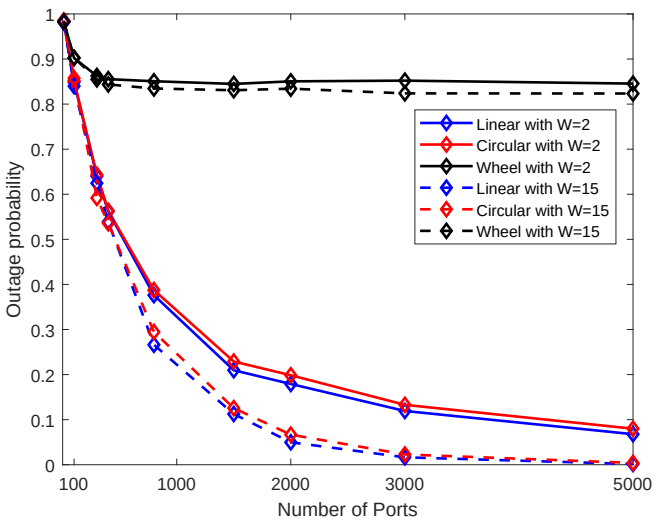

Fig. 7: Outage probability versus the number of ports by considering different fluid antennas architectures, when $D_0 =$ 10m and $U = 6$.

Fig. 7 illustrates the outage probability versus the number of ports N. As expected, the outage probability decreases as N increases for both linear and circular topologies, which indicates that both the performance are improved as N increases. Among these three topologies, the wheel topology performs the poorest performance. For the wheel topology, with the increase of N, there is an initial descent observed in the outage probability. Nonetheless, subsequent to this phase, the influence of N on the outage probability becomes negligible. This is because the d_k of the wheel topology is always constant when we increase N. Consequently, all ports within the wheel topology continue to encounter identical channel characteristics, thereby resulting in a near-consistent performance level. Moreover, as expected, one can see that the performance of all three topologies is improved as we increase the size W of the fluid antenna. In particular, if $W = 15$, a nearly negligible outage probability can be achieved with 3000 ports.

Fig. 8 and Fig. 9 depicts the outage probability and the multiplexing gain versus the number of users under different SNR Γ. As expected, the outage probability increases with the number of users. Moreover, a notable enhancement in antenna performance can be observed for all three topologies, when the SNR increases from 5 dB to 10 dB. Among the three topologies, the wheel topology antenna exhibits the most pronounced improvement. However, its performance is still worse than the other two topologies.

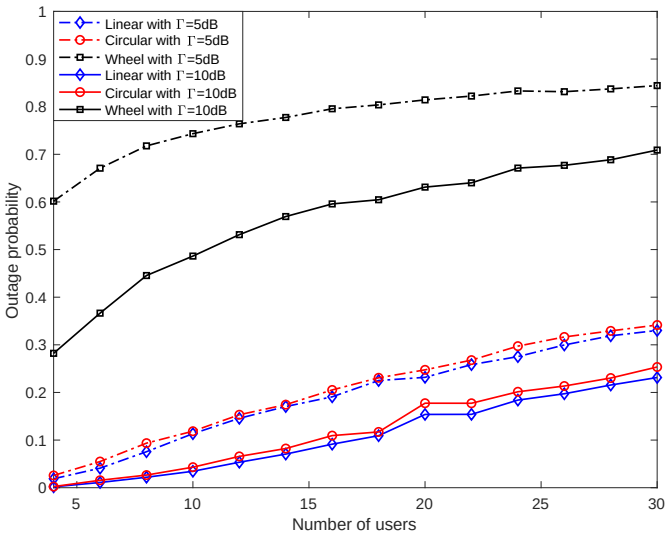

Fig. 8: Outage probability versus the number of users by considering different fluid antennas architectures and SNR Γ, where $W = 15$, $N = 600$ and $D_0 = 10$m.

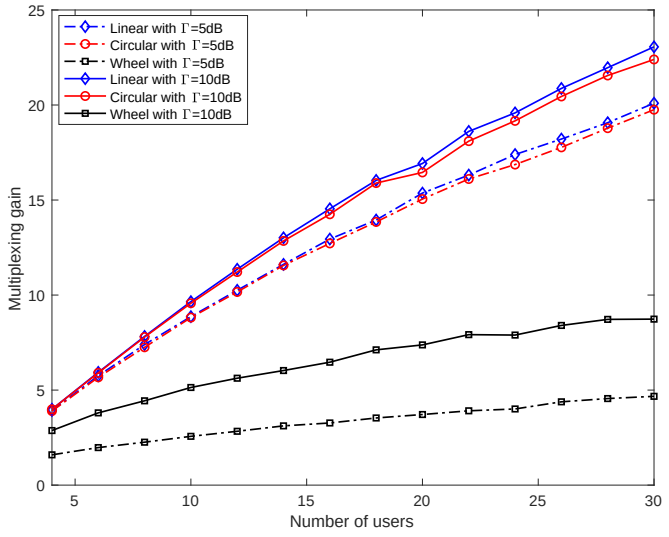

Fig. 9: Multiplexing gain versus the number of users by considering different fluid antennas architectures and SNR Γ, where $W = 15$, $N = 600$ and $D_0 = 10$m.

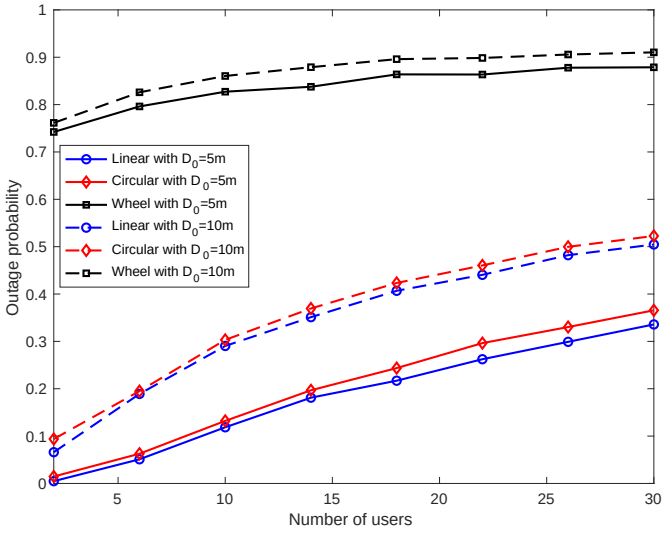

Fig. 10: Outage probability versus the number of users by considering different fluid antennas architectures and setting different reference distance D_0, where $N = 600$ and $W = 15$.

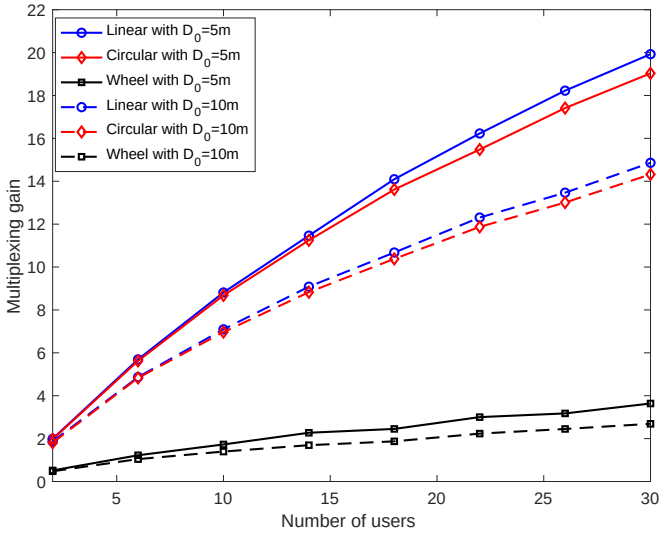

Fig. 11: Multiplexing gain versus the number of users by considering different fluid antennas architectures and setting different reference distance D_0, where $N = 600$ and $W = 15$.

Fig. 10 and Fig. 11 illustrate the outage probability and the multiplexing gain versus the number of users, by considering different fluid antennas architectures, respectively. Observe from Fig. 11 that the multiplexing gain is significantly higher when the transmitter is closer to the antenna (i.e., $D_0 = 5$m) compared to the case when the transmitter is farther away from the antenna (i.e., $D_0 = 10$m) for both linear and circular topologies. However, the difference of multiplexing gain for the wheel topology antenna at the two distances is much smaller. Similarly, the outage probability is significantly smaller when the transmitter is closer to the antenna (i.e., $D_0 = 5$m) compared to when the transmitter is farther away from the antenna (i.e., $D_0 = 10$m) for both linear and circular topologies. In contrast, the difference in the performance of the wheel topology antenna at the two distances is much smaller. Among these three topologies, the wheel topology perform the poorest performance, while the linear and circular shapes perform similarly. This is because the d_k of the wheel topology is constant, resulting in all ports experiencing the same channel characteristic, eliminating any channel selection advantage. This confirms the importance of choosing different antenna topologies for different situations.

V. Conclusion

A new f-FAMA channel model is proposed in this paper, which considers the path loss difference among different ports on the FAS. By adopting the new channel model, the performance of different fluid antenna architectures was then analysed. Simulation results show that path loss does have a significant impact on the outage probability and multiplexing gain, with the outage probability of the path loss model being higher when subsequent ports are getting further away from the transmit antenna. Furthermore, it can be observed that for the case of $U < 5$, the performance of the linear and circular architecture is similar. When $U \geq 5$, the linear architecture outperforms the circular architecture. It can also be observed that by using the current performance metrics, the wheel architecture is not very suitable to be adopted when the power signal is small, while the linear architecture has the best overall performance.

References

[1] N. H. Mahmood et al., White paper on critical and massive machine type communication towards 6G [White paper], (6G Research Visions, No. 11). University of Oulu. [Online] http://urn.fi/urn:isbn:9789526226781.

[2] A. Ghosh, A. Maeder, M. Baker and D. Chandramouli, 5G evolution: A view on 5G cellular technology beyond 3GPP Release 15, IEEE Access, vol. 7, pp. 127639C127651, 2019.

[3] E. G. Larsson, O. Edfors, F. Tufvesson and T. L. Marzetta, "Massive MIMO for next generation wireless systems," in IEEE Communications Magazine, vol. 52, no. 2, pp. 186-195, February 2014, doi: 10.1109/MCOM.2014.6736761.

[4] L. Zhu, Z. Xiao, X.-G. Xia and D. Oliver Wu, Millimeter-wave communications with non-orthogonal multiple access for B5G/6G, IEEE Access, vol. 7, pp. 116123C116132, 2019.

[5] A. Grau Besoli and F. De Flaviis, A multifunctional reconfigurable pixeled antenna using MEMS technology on printed circuit board, IEEE Trans. Antennas & Propag., vol. 59, no. 12, pp. 4413C4424, Dec. 2011.

[6] S. Song and R. D. Murch, An efficient approach for optimizing frequency reconfigurable pixel antennas using genetic algorithms, IEEE Trans. Antennas & Propag., vol. 62, no. 2, pp. 609C620, Feb. 2014.

[7] B. A. Cetiner et al., Multifunctional reconfigurable MEMS integrated antennas for adaptive MIMO systems, IEEE Commun. Mag., vol. 42, no. 12, pp. 62C70, Dec. 2004.

[8] Y. Huang, L. Xing, C. Song, S. Wang and F. Elhouni, Liquid antennas: Past, present and future, IEEE Open J. Antennas and Propag., vol. 2, pp. 473C487, 2021.

[9] A. M. Morishita, C. K. Y. Kitamura, A. T. Ohta, and W. A. Shiroma, A liquid-metal monopole array with tunable frequency, gain, and beam steering, IEEE Antennas Wireless Propag. Lett., vol. 12, pp. 1388C1391, 2013.

[10] C. Borda-Fortuny, K.-F. Tong, A. Al-Armaghany, and K. K. Wong, A low-cost fluid switch for frequency-reconfigurable Vivaldi antenna, IEEE Antennas Wireless Propag. Lett., vol. 16, pp. 3151C3154, 2017.

[11] K. K. Wong, A. Shojaeifard, K. F. Tong, and Y. Zhang, Fluid antenna systems, IEEE Trans. Wireless Commun., vol. 20, no. 3, pp. 1950C1962, Mar. 2021.

[12] M. Khammassi, A. Kammoun, and M.-S. Alouini, A new analytical approximation of the fluid antenna system channel, [Online] arXiv preprint arXiv:2203.09318, 2022.

[13] C. Psomas, G. M. Kraidy, K. K. Wong, and I. Krikidis, On the diversity and coded modulation design of fluid antenna systems, [Online] arXiv preprint arXiv:2205.01962, 2022.

[14] P. Mukherjee, C. Psomas, and I. Krikidis, On the level crossing rate of fluid antenna systems, [Online] arXiv preprint arXiv:2205.01711, 2022.

[15] L. Tlebaldiyeva, G. Nauryzbayev, S. Arzykulov, A. Eltawil, and T. Tsiftsis, Enhancing QoS through fluid antenna systems over correlated Nakagami-m fading channels, in Proc. IEEE Wireless Commun. & Netw. Conf. (WCNC), pp. 78C83, 10-13 Apr. 2022, Austin, TX, USA.

[16] K. K. Wong, A. Shojaeifard, K. -F. Tong and Y. Zhang, "Performance Limits of Fluid Antenna Systems," in IEEE Communications Letters, vol. 24, no. 11, pp. 2469-2472, Nov. 2020, doi: 10.1109/LCOMM.2020.3006554.

[17] C. Skouroumounis and I. Krikidis, Fluid antenna with linear MMSE channel estimation for large-scale cellular networks, to appear in IEEE Trans. Commun., 2023.

[18] K. K. Wong, and K. F. Tong, Fluid antenna multiple access, IEEE Trans. Wireless Commun., vol. 21, no. 7, pp. 4801C4815, Jul. 2022.

[19] K. K. Wong, D. Morales-Jimenez, and K. F. Tong, Slow fluid antenna multiple access, submitted to IEEE Trans. Commun., 2022.

[20] K. -K. Wong, K. -F. Tong, Y. Chen and Y. Zhang, "Fast Fluid Antenna Multiple Access Enabling Massive Connectivity," in IEEE Communications Letters, vol. 27, no. 2, pp. 711-715, Feb. 2023, doi: 10.1109/LCOMM.2022.3222574.

[21] H. Yang, K. -K. Wong, K. -F. Tong, Y. Zhang and C. -B. Chae, "Performance Analysis of Slow Fluid Antenna Multiple Access in Noisy Channels Using Gauss-Laguerre and Gauss-Hermite Quadratures," in IEEE Communications Letters, vol. 27, no. 7, pp. 1734-1738, July 2023, doi: 10.1109/LCOMM.2023.3275054.

[22] M. K. Samimi, T. S. Rappaport and G. R. MacCartney, "Probabilistic Omnidirectional Path Loss Models for Millimeter-Wave Outdoor Communications," in IEEE Wireless Communications Letters, vol. 4, no. 4, pp. 357-360, Aug. 2015, doi: 10.1109/LWC.2015.2417559.

[23] G. Durgin, T. S. Rappaport and H. Xu, "5.85-GHz radio path loss and penetration loss measurements in and around homes and trees," in IEEE Communications Letters, vol. 2, no. 3, pp. 70-72, March 1998, doi: 10.1109/4234.662630.